

CT angiography in the diagnosis of cardiovascular disease: a transformation in cardiovascular CT practice

Zhonghua Sun¹, Mansour Al Moudi², Yan Cao³

¹Discipline of Medical Imaging, Department of Imaging and Applied Physics, Curtin University, Perth, 6102, Western Australia, Australia;

²Department of Medical Imaging and Nuclear Medicine, King Saud Medical City, Riyadh, Saudi Arabia; ³Department of Medical Imaging, Shandong Medical College, Jinan 276000, China

Correspondence to: Associate Professor Zhonghua Sun. Discipline of Medical Imaging, Department of Imaging and Applied Physics, Curtin University, Perth, 6102, Australia. Email: z.sun@curtin.edu.au.

Abstract: Computed tomography (CT) angiography represents the most important technical development in CT imaging and it has challenged invasive angiography in the diagnostic evaluation of cardiovascular abnormalities. Over the last decades, technological evolution in CT imaging has enabled CT angiography to become a first-line imaging modality in the diagnosis of cardiovascular disease. This review provides an overview of the diagnostic applications of CT angiography (CTA) in cardiovascular disease, with a focus on selected clinical challenges in some common cardiovascular abnormalities, which include abdominal aortic aneurysm (AAA), aortic dissection, pulmonary embolism (PE) and coronary artery disease. An evidence-based review is conducted to demonstrate how CT angiography has changed our approach in the diagnosis and management of cardiovascular disease. Radiation dose reduction strategies are also discussed to show how CT angiography can be performed in a low-dose protocol in the current clinical practice.

Keywords: Cardiovascular disease; computed tomography angiography (CTA); diagnosis; visualisation

Submitted Sep 19, 2014. Accepted for publication Sep 26, 2014.

doi: 10.3978/j.issn.2223-4292.2014.10.02

View this article at: <http://dx.doi.org/10.3978/j.issn.2223-4292.2014.10.02>

Introduction

Over the last two decades, cardiac computed tomography (CT) has witnessed significant developments in the diagnosis of cardiovascular disease, owing to the technical improvements in CT imaging, which allows rapid data acquisition with high spatial resolution. CT angiography (CTA) has been widely used in the diagnostic evaluation of many cardiovascular diseases, and this technique currently serves as the first line modality in the early diagnosis of abdominal aortic aneurysm (AAA), aortic dissection and pulmonary embolism (PE) (1-5). Coronary CT angiography (CCTA) represents one of the most important technical advancements in cardiovascular CT practice, and it is becoming a standard clinical assessment for patients with low to intermediate pre-test probability for coronary artery disease (6-15). CTA is also commonly used to follow-up patients treated with endovascular stents and stent grafts

with the aim of determining stent and stent graft patency, stent graft-related complications (16-20).

Despite significant improvements in cardiovascular CT practice, CTA still remains a challenging procedure in routine clinical practice due to the following reasons: first, acquisition of optimal image quality remains an issue in CCTA, as heart rate control with appropriate electrocardiogram (ECG)-gating and good time of contrast injection comprises an essential component of CTA. Second, radiation dose associated with CTA is a medical concern; although significant progress has been made in reducing radiation dose with the use of dose-saving strategies, with resultant dose value similar to or even lower than invasive coronary angiography (21). However, a collaborative team between skilled medical imaging technologists and physicians play an important role in achieving such a low-dose protocol with diagnostic quality images, since

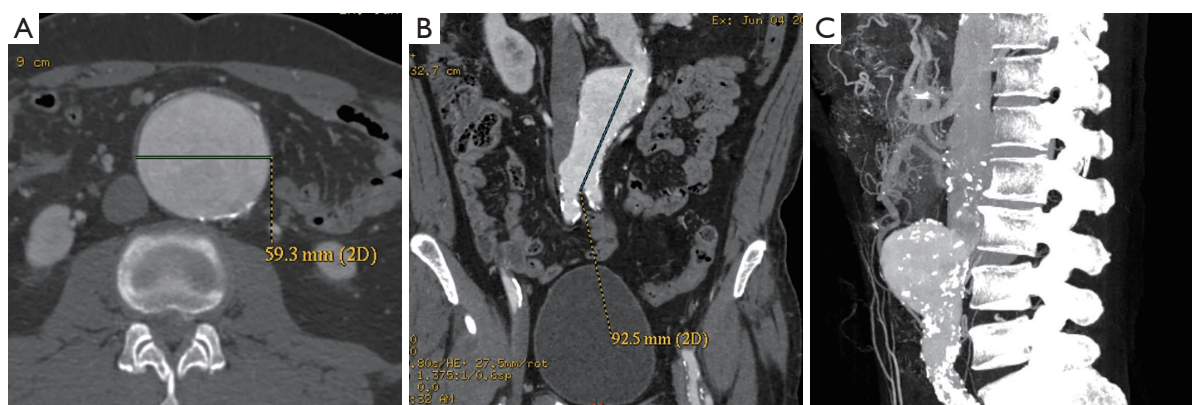


Figure 1 Measurements of aortic aneurysm diameter and aneurysm extent in relation to the aortic branches. (A) 2D axial CT shows maximal abdominal aortic aneurysm diameter of 59.3 mm; (B) coronal multiplanar reformation shows aneurysm extent of 92.5 mm, ranging from the proximal to distal segments of the aneurysm; (C) sagittal maximum-intensity projection demonstrates an infrarenal aortic aneurysm with extensive calcifications in the arterial wall. CT, computed tomography; 2D, two-dimensional.

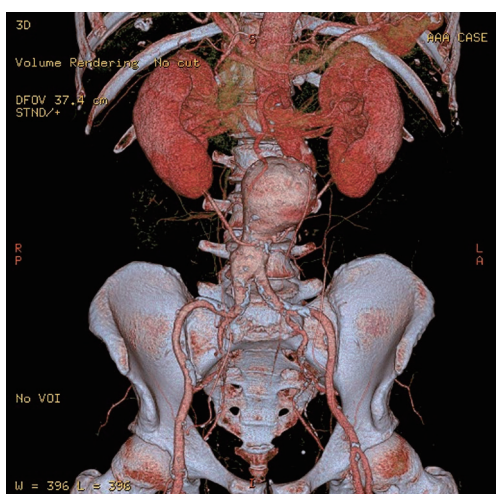


Figure 2 3D volume rendering shows an infrarenal aortic aneurysm in relation to the renal arteries and common iliac arteries. 3D, three-dimensional.

suboptimal scanning techniques or inappropriate referral protocols result in suboptimal image quality and high radiation dose.

This review provides an overview of the diagnostic application of CTA in cardiovascular CT practice with a focus on the diagnostic accuracy of CTA in the common cardiovascular disease, including AAA, aortic dissection and PE. CTA in the assessment of endovascular stent graft repair of aortic aneurysm and aortic dissection is also reviewed. More attention is paid to the CCTA in the diagnosis of

coronary artery disease with regard to the diagnostic and prognostic value of this rapidly evolved technique. Finally, recently introduced capabilities for CCTA such as fractional flow reserve (FFR) CT and effective dose reduction through iterative reconstruction (IR) are highlighted.

CTA in AAA and endovascular stent graft repair

With rapid technical developments in CT imaging technique, in particular, the widespread use of multislice CT, CTA has become a routine imaging modality in the diagnostic evaluation of patients with AAA, while invasive angiography is only reserved for solving complications situations where CTA shows indeterminate results.

CTA imaging of abdominal aorta, aneurysm and relationship between the aneurysm and aortic branches has been complemented by a number of two-dimensional (2D) and 3D reconstruction visualisations which enhances the diagnostic value of CTA to a greater extent (22-27). In addition to the routinely viewed 2D axial images (*Figure 1A*), multiplanar reformation (MPR) CTA images are generated for measurement of aneurysm length in relation to the proximal and distal aneurysm necks (*Figure 1B*), while maximum-intensity projection (MIP) is commonly used to demonstrate the extent of aneurysm in relation to the aortic branches (*Figure 1C*). 3D volume rendering technique (VRT) provides volumetric information of the aneurysm and other structures as shown in *Figure 2*. Measurement of proximal aneurysm neck length between the renal arteries and aneurysm plays an important role in pre-operative planning

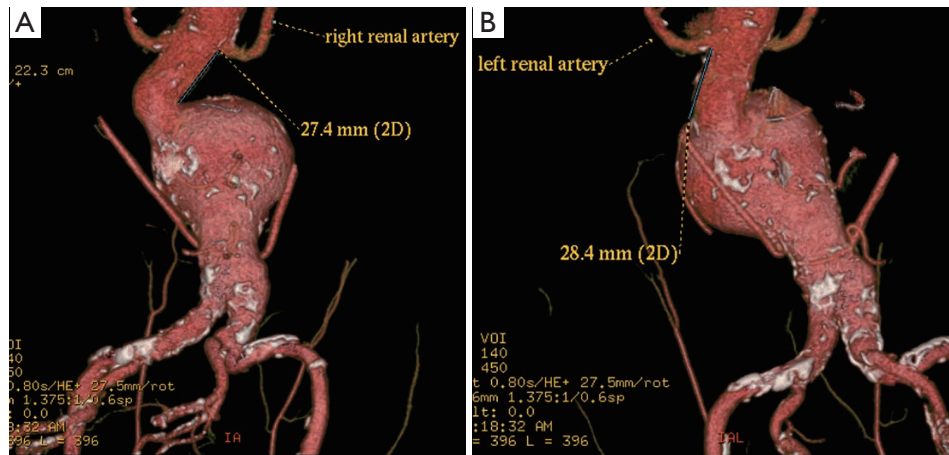


Figure 3 3D volume rendering shows measurement of the distance between the right (A) and left renal arteries (B) and the proximal segment of the aneurysm. 3D, three-dimensional.

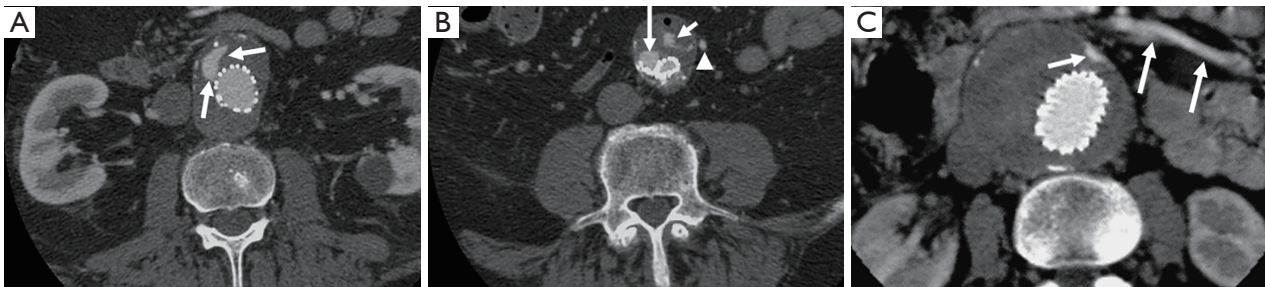


Figure 4 A type I endoleak is present in the proximal and distal segments of aortic stent graft, as demonstrated on the axial CT images (long arrows in A and B). A type II endoleak (short arrow in B) is also noticed within the aneurysm sac at the level of common iliac artery due to patent inferior mesenteric artery (arrowhead in B). A type II endoleak (short arrows) is present in the anterior aspect of an aortic aneurysm following endovascular repair due to backfilling from the patent inferior mesenteric artery (long arrows) (C). CT, computed tomography.

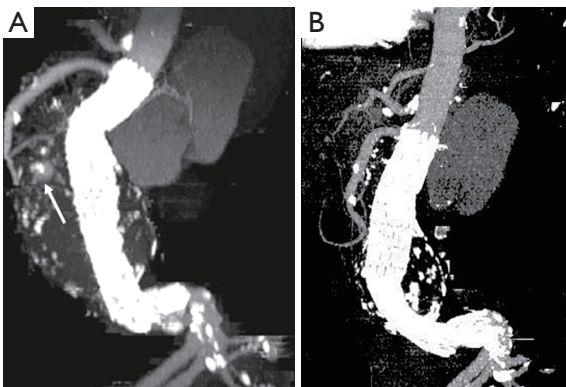


Figure 5 (A) A 74-year-old man had stent migration of 10.2 mm due to foreshortening of the longitudinal aneurysm sac at the 24-month follow-up (B). The arrow in A indicates a type II endoleak, which resolved spontaneously. Reprint with permission from ref (40).

of endovascular aneurysm repair (EVAR) (Figure 3).

While open surgical repair of AAA is still commonly performed, EVAR has been increasingly used in many clinical centres due to its less invasiveness, lower procedure-related complications compared to open surgery (28-30). EVAR has been reported to be especially suitable for patients with comorbid medical conditions such as cardiac disease, chronic obstructive pulmonary disease, diabetes, renal disease, cerebrovascular disease or peripheral artery disease (31,32). Stent-graft integrity is of paramount importance to EVAR of AAA, and this can only be assessed by medical imaging. Currently, CTA is the preferred imaging modality for routine imaging follow-up of postoperative EVAR (16-19). CTA follow-up of EVAR includes measurements of aneurysm diameter to determine aneurysm sac size change (33-35), detection of stent graft-related complications such as endoleaks (Figure 4), which is the most commonly

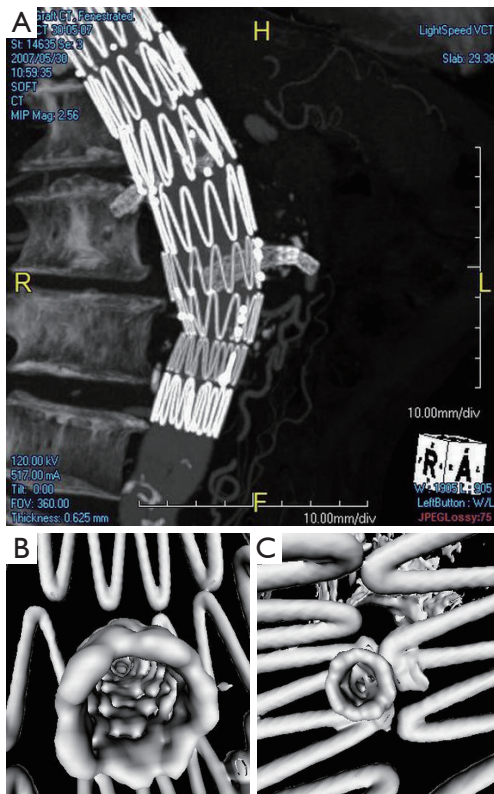


Figure 6 (A) CT angiography-generated maximum-intensity projection shows renal stents in bilateral renal arteries in a patient treated with fenestrated stent grafting; (B,C) corresponding virtual intravascular endoscopy reveals intraluminal appearance of the renal stents which are smooth and circular. CT, computed tomography.

reported occurrence following EVAR (36-39), and stent graft migration (Figure 5) (40,41).

Another 3D visualisation tool generated from CTA is virtual intravascular endoscopy (VIE) which shows unique intraluminal views of the aortic wall as well as stent wires (42-45). Studies have shown that VIE allows demonstration of intraluminal appearances of stent grafts (Figure 6), in particular the relationship between stent wires and renal artery ostia (Figure 7). This is clinically significant as the long-term outcomes of EVAR still remains to be understood, thus, VIE serves as a complementary tool to conventional CTA-generated visualisations for accurate assessment of treatment outcomes of EVAR (42-46).

CTA in aortic dissection

CTA or echocardiography is usually performed in patients

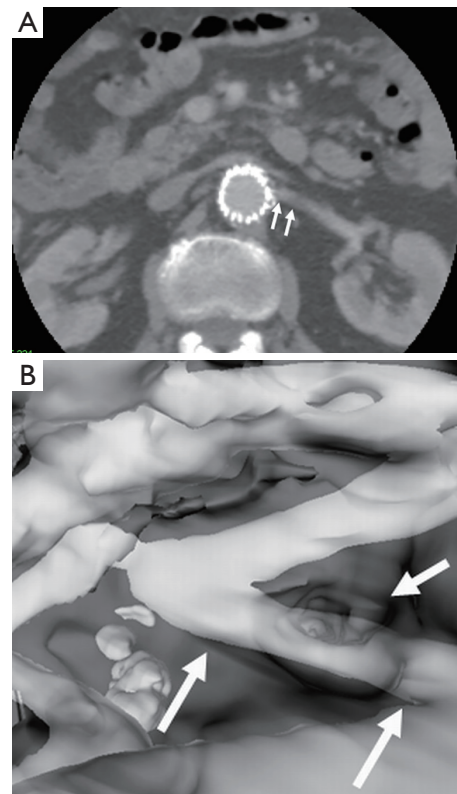


Figure 7 2D axial CT image shows that suprarenal stent graft is placed above the left renal artery (arrows in A) in a patient treated with suprarenal aortic stent-graft. Corresponding virtual intravascular endoscopy confirms that the left renal ostium is crossed by a single stent wire (B). Short arrow in B indicates the renal ostium, while long arrows refer to the suprarenal stent wires. 2D, two-dimensional; CT, computed tomography.

with suspected acute aortic dissection based on clinical presentation and initial investigations (47-50). A systematic review of the diagnostic value of CTA, transesophageal echocardiography, and magnetic resonance imaging (MRI) reported that the mean sensitivity and specificity was more than 95% for all three examinations (51). Although MRI was found to be slightly superior to the other two modalities in patients with high pretest probability of aortic dissection, CTA is the preferred imaging modality in patients with low or intermediate pretest probability of aortic dissection; in particular, CT is widely available in the emergency department (47).

CTA-generated axial CT imaging supplemented by 2D or 3D reconstructions is able to identify the intimal flap which separates the true lumen from the false lumen, the size of true and false lumen (Figure 8), localization of the



Figure 8 Sagittal reformatted CT angiography shows Stanford type A aortic dissection with true lumen (short arrows) compressed by the false lumen. Aortic dissection arises from the ascending aorta as indicated by the large arrows. CT, computed tomography.

intimal tear, extent of aortic dissection with regard to the involvement of aortic branches (*Figure 9*), and the presence of hematoma, mediastinal hematoma or pleural effusion (52).

Conventional CTA without ECG-gating allows for acquisition of static images of intimal flap, thus reflects the configuration of the intimal flap at an arbitrary time point. However, motion artifacts of the ascending aorta or of an intimal flap can cause cardiac pulsation, thus affecting image quality in aortic dissection (53). ECG-gated CTA is therefore recommended for evaluation of aortic dissection as it allows the phase-resolved cine imaging by eliminating the impact of motion artifacts due to cardiac pulsation (54), and the 4D images enable assessment of the dynamics of the intimal flap movement during a cardiac cycle (55-57). Studies reported that ECG-gated CTA can assess the intimal flap motion by demonstrating the actual status of true and false lumen during cardiac cycle (*Figure 10*), thus, providing more information about true lumen collapse. Identification of pulsating and static types of aortic dissection with ECG-gated CTA is considered useful for differentiation of unstable aortic dissection from stable one (55,58).

The management of an aortic dissection depends on the type, time course, and symptoms associated with the dissection. Acute Stanford type A aortic dissection represents

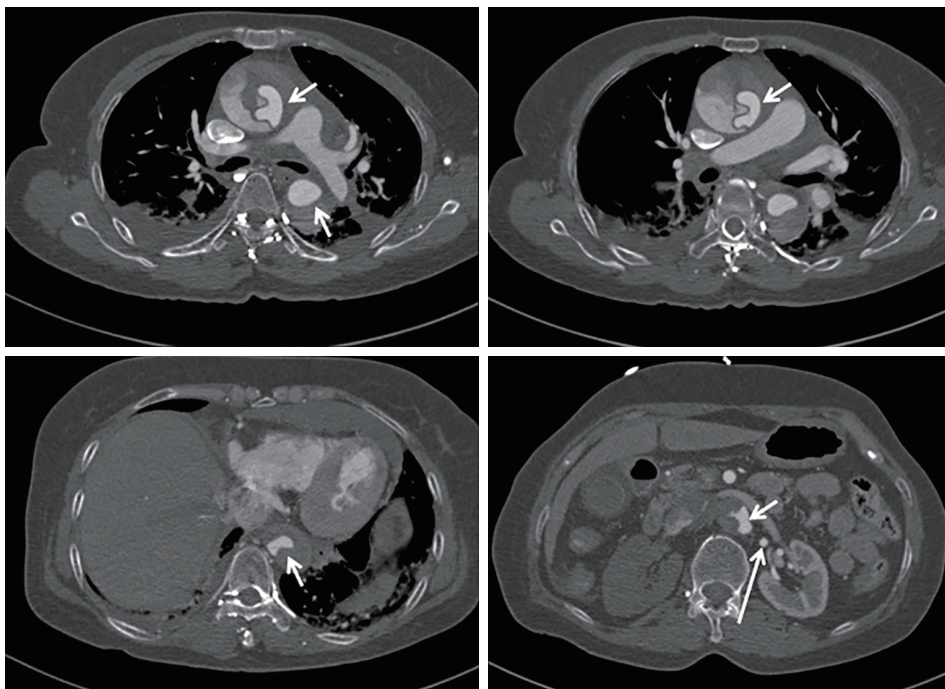


Figure 9 2D axial images of CT angiography show Stanford type A aortic dissection extending from the ascending aorta to the abdominal aorta with true lumen (short arrows) much smaller than the false lumen. The left renal artery (long arrow) arises from the true lumen. 2D, two-dimensional; CT, computed tomography.

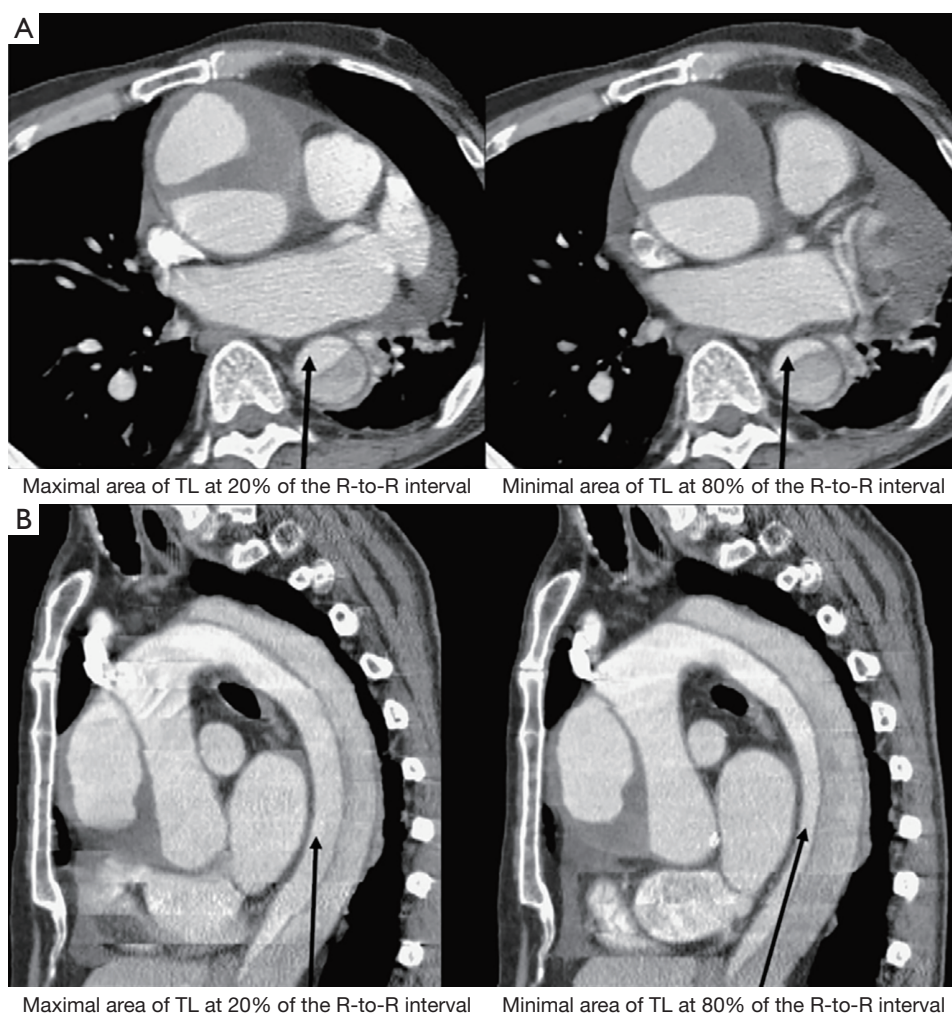


Figure 10 (A) Typical axial source images of a subject with aortic dissection in which true lumen (TL) becomes maximal at 20% of the R-to-R interval of the electrocardiogram (left) and TL becomes minimal at 80% of the R-to-R interval (right); (B) typical multiplanar reconstruction images from the left anterior oblique view of a subject with aortic dissection in which TL becomes maximal at 20% of the R-to-R interval of the electrocardiogram (left) and TL becomes minimal at 80% of the R-to-R interval (right). Reprint with permission from ref (55).

a surgical emergency, and it is managed by surgical repair, while management of Stanford type B dissection is determined by the situation whether the dissection is complicated or not. Due to invasiveness and high mortality associated with surgical repair, endovascular stent grafting is increasingly used as a less invasive alternative to treat complicated type B dissection (59). CTA is used as a routine imaging modality for follow-up of endovascular repair of aortic dissection by showing the stent graft in relation to the aortic branches (*Figure 11*), stent grafts or stents position in the aorta (*Figure 12*), and volumetric changes in the true and false lumen (*Figure 13*) (60,61).

CTA in PE

CT pulmonary angiography (CTPA) has been widely recognized as the method of choice for diagnosis of suspected PE due to its superior sensitivity and specificity to ventilation-perfusion (V/Q) radioisotope scanning (62,63). The main advantages of CTPA over V/Q scans in PE include higher diagnostic accuracy, faster acquisition time with high contrast images, and readily availability at many clinical centres (64). The wide availability and high diagnostic performance have led to the increasing use of CTPA as the first line modality to detect or exclude PE

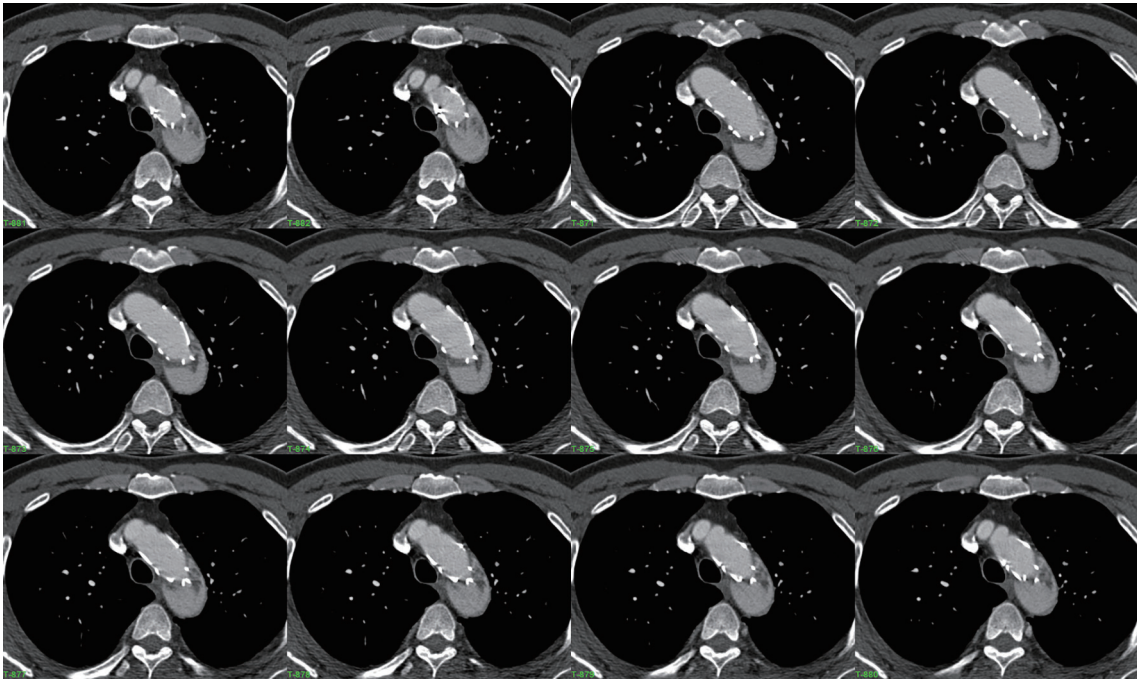


Figure 11 A series of 2D axial images in a patient with Stanford type B aortic dissection treated with endovascular stent graft show that the stent graft is placed in the ascending aorta, just below the left subclavian artery. 2D, two-dimensional.

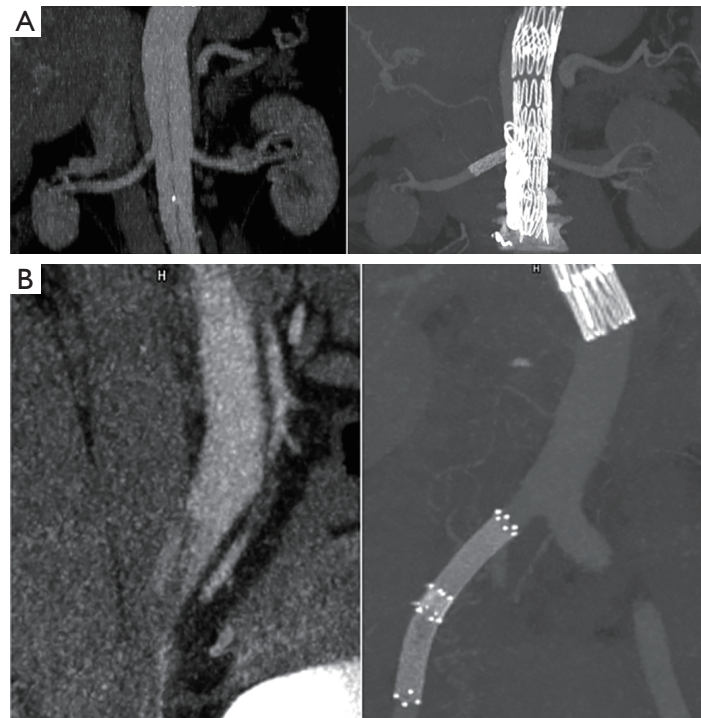


Figure 12 Adjunctive stent placement during the initial procedure. (A) The right renal artery originally perfused by the false lumen (left panel) was treated with a stent inserted from the true lumen through the uncovered dissection stent (right panel). This patient also underwent coil embolization of the distal false lumen and a lumbar artery; (B) the dissected right common iliac artery (left panel) was treated with placement of two stents (right panel). Reprint with permission from ref (60).

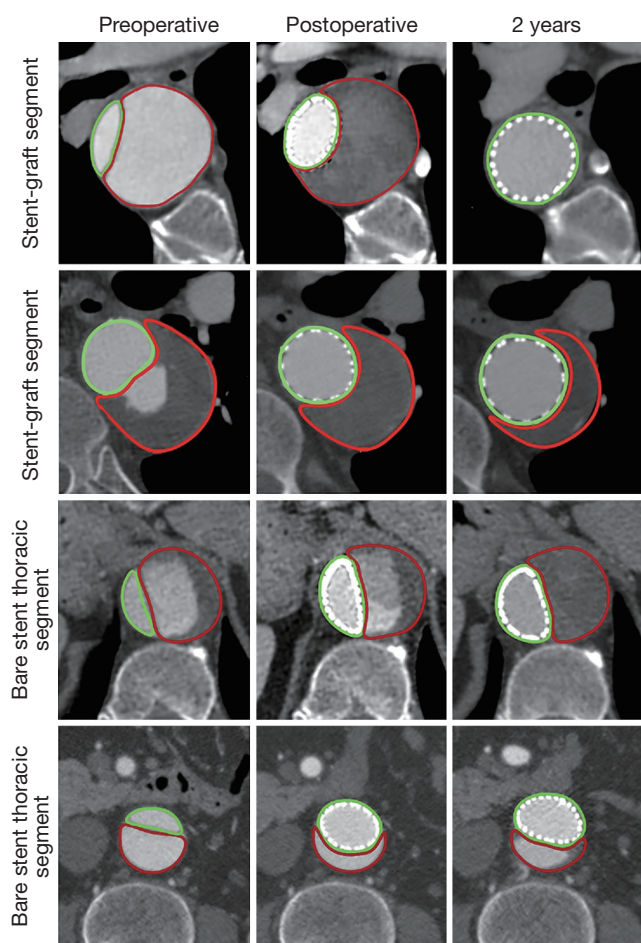


Figure 13 True lumen (TL, green) and false lumen (FL, red) were selected separately from the innominate artery to the aortic bifurcation for all follow-up CT scans and compared with preoperative examinations. This example demonstrated the behavior over the time of lumina in the different aortic segment after treatment with the endovascular stent grafting technique. Reprint with permission from ref (61). CT, computed tomography.

both in the emergency department and in-patient setting.

The use of CTPA as a reliable diagnostic imaging modality to exclude PE has been confirmed by clinical trials (65,66). A meta-analysis of safety of ruling out PE by CTPA showed that a normal CTPA alone can safely exclude PE in all patients in whom CTPA is required to rule out PE, with pooled 3-month venous thromboembolism rate for patients with a normal CTPA being 1.2% (95% confidence interval: 0.8-1.8%) (67).

Technical improvements in multislice CT allow accurate detection of PE, in particular subsegmental PE. A meta-

analysis shows that the rate of isolated subsegmental PE detected by multislice CTPA is twice as high when compared to that used by single slice CTPA (68). Despite high radiation dose associated with CTPA, it still remains the most reliable imaging modality for detection of PE. The PIOPED III study reported that MR pulmonary angiography (MRPA) has a sensitivity of 78% and a specificity of 99% compared to CTPA and V/Q scans, which are regarded as the reference standard (69). Furthermore, MRPA was technically inadequate in 25% of the patients. Similar diagnostic value of MRPA was reported in another study with similar percentage of inconclusive results due to technical reasons (70).

For visualization of the pulmonary embolism with CTPA, 2D axial and multiplanar reformation images are the most commonly used visualization tools for detection of segmental and subsegmental PE (Figure 14). Others postprocessing tools are also available to evaluate the CTPA datasets, which include MIP, and VTR (71,72) (Figure 15).

CCTA in coronary artery disease

Increasing evidence shows that CCTA is a well-established imaging modality in the diagnosis of coronary artery disease due to its less invasiveness, high diagnostic value, and widespread accessibility (7-10,73-77). Expansion of multislice CT systems from a 64- to 320-slice system has allowed for the accurate assessment of stenosis severity and atherosclerotic plaque composition (Figure 16) (78), or even the acquisition of whole-heart coverage in one gantry rotation (15). Systematic reviews and meta-analyses reported the high diagnostic accuracy of 320-slice CCTA, with sensitivity similar to that observed in 64-slice CCTA, but specificity higher than in 64-slice CCTA (79,80). Although extended z-axis coverage is improved with use of 320-slice CCTA, temporal resolution of 320-slice CT is inferior to that of 64- or 128-slice CT, thus, heart rate control is still necessary in most of CCTA examinations (81). Table 1 summarizes the diagnostic value of these studies performed with 64- and 320-slice CCTA in coronary artery disease.

In addition to the excellent diagnostic performance in coronary artery disease, CCTA also shows high prognostic value in the prediction of major adverse cardiac events. A direct correlation between CCTA findings and the occurrence of future cardiac events has been reported by studies based on short-term to long-term follow-up, with results showing that normal CCTA is associated with a very

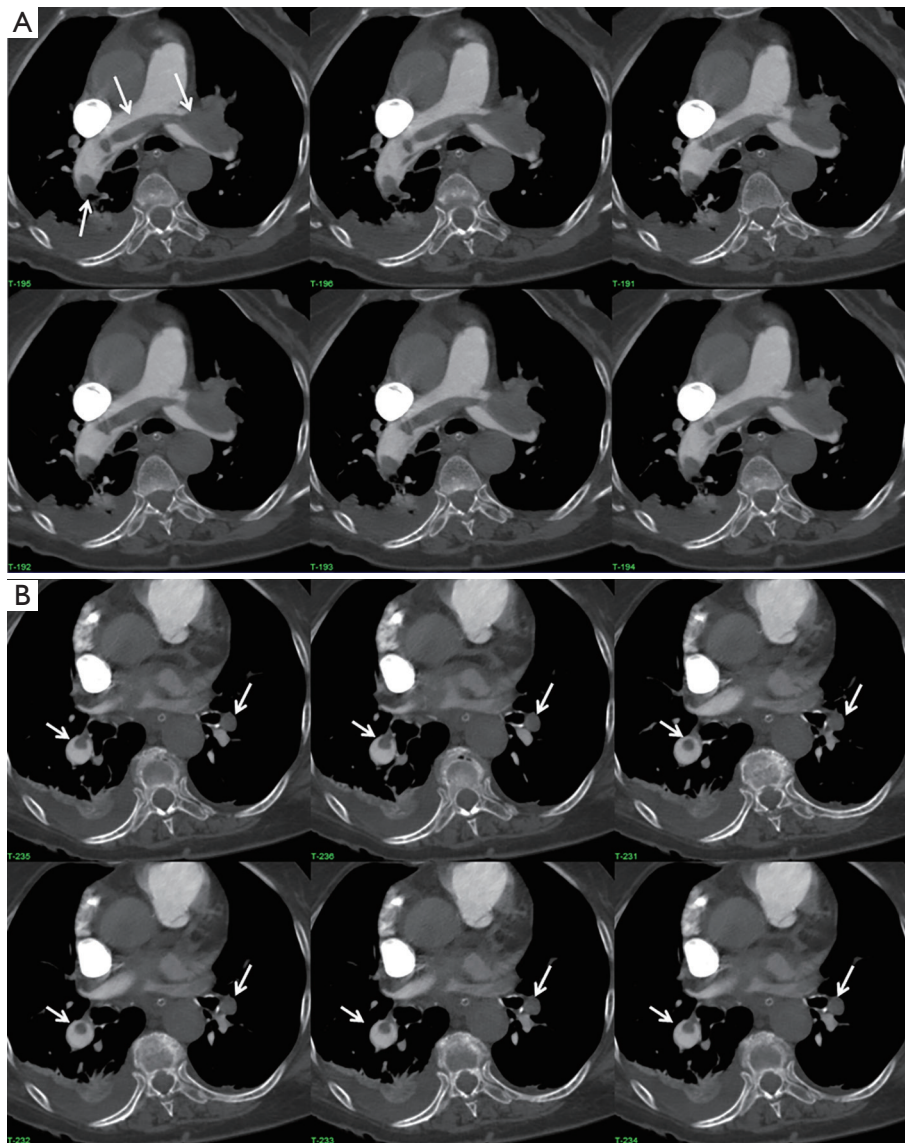


Figure 14 (A) 2D axial CT images show pulmonary embolism located in the main pulmonary trunk, with involvement of bilateral main pulmonary arteries (arrows); (B) the same patient as A, pulmonary embolism extends to the segmental branches (arrows). 2D, two-dimensional; CT, computed tomography.

low rate of adverse cardiac events (<1%), while in patients with obstructive coronary artery disease, the event rate is significantly higher (3-59%) (82-91) (Figure 17). These results indicate that CCTA could serve as an independent predictor of major adverse cardiac events in patients with suspected coronary artery disease, although multicentre studies with long-term follow-up are required since most of the currently reports are based on single centres' experience with short to mid-term follow-up.

In recent years, there has been an increasing interest

in the investigation of diagnostic performance of non-invasive FFR derived from CCTA (FFRCT). Computation of FFRCT is performed by computational fluid dynamics (CFD) modelling after segmentation of coronary arteries and left ventricular myocardium. The FFRCT ratio is obtained by dividing the mean pressure distal to the coronary stenosis by the mean aortic pressure, which can be measured during CFD simulations. An FFR of ≤ 0.80 is currently used as a cut off value to determine coronary stenoses responsible for ischemia (Figures 18,19) (92,93).

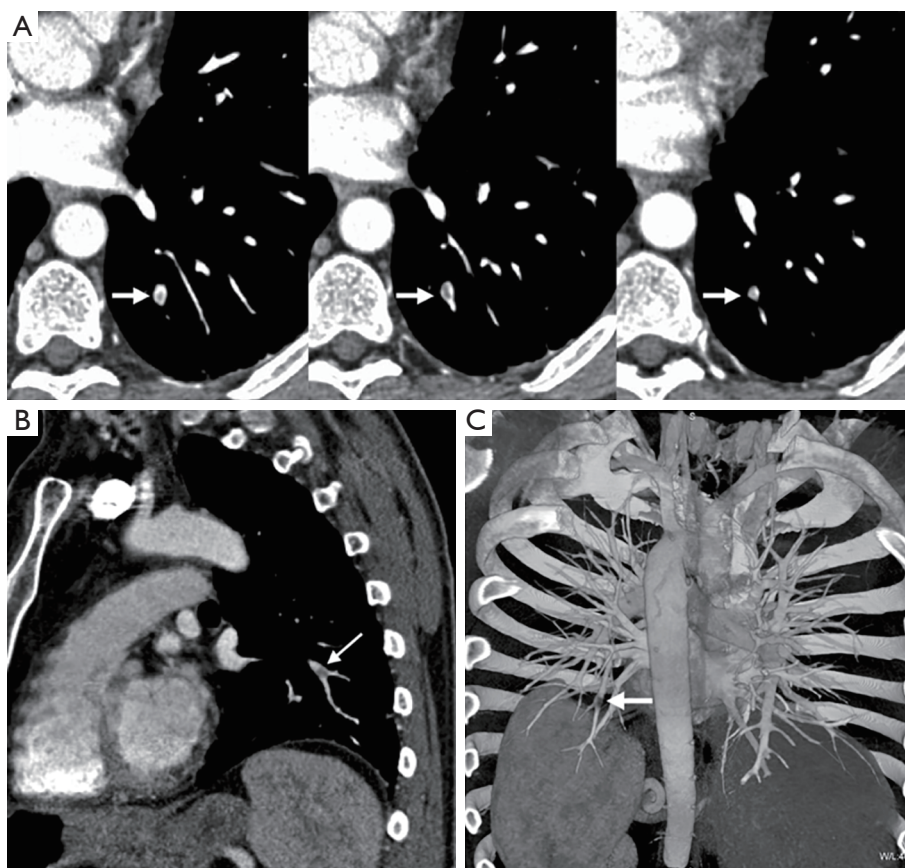


Figure 15 CT pulmonary angiography in a 57-year-old man with mild pleuritic chest pain. (A) Consecutive transverse sections show isolated peripheral pulmonary embolus (arrows) in a subsegmental pulmonary artery in segment 9 of the left lung; (B) oblique sagittal multiplanar reformation also shows embolus (arrow); (C) coronal volume-rendered display (posterior view) shows isolated peripheral filling defect (arrow) in otherwise normal pulmonary vascular tree. Reprint with permission from ref (72). CT, computed tomography.

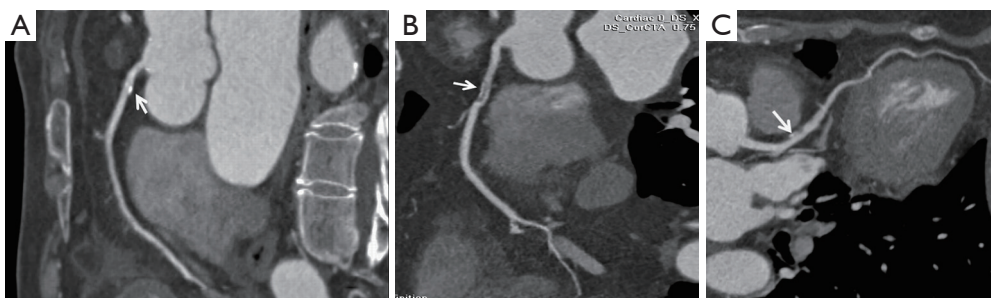


Figure 16 Coronary CT angiography characterization of plaque composition. (A) A calcified plaque (arrow) is seen in the proximal segment of right coronary artery in a 65-year-old woman with suspected coronary artery disease; (B) a non-calcified plaque (arrow) is detected in the proximal segment of right coronary artery in a 67-year-old woman with known coronary artery disease; (C) a mixed plaque (arrow) is observed in the proximal segment of left anterior descending coronary artery in a 55-year-old female with suspected coronary artery disease. CT, computed tomography.

Table 1 Diagnostic value of coronary CT angiography in coronary artery disease according to systematic reviews and meta-analyses

Type of CT scan	First author	No. of articles in the analysis	Patient-based sensitivity % [95% CI]	Patient-based specificity % [95% CI]
64-slice coronary CT angiography	Abdulla <i>et al.</i> 2007 (9)	27	97.5 [96-99]	91 [87.5-94]
	Stein <i>et al.</i> 2008 (10)	23	98 [96-98]	88 [85-89]
	Mowatt <i>et al.</i> 2008 (11)	28	99 [97-99]	89 [83-94]
	Sun <i>et al.</i> 2008 (7)	15	97 [94-99]	88 [79-97]
	Guo <i>et al.</i> 2011 (14)	24	98 [99-99]	87 [83-90]
	Salavati <i>et al.</i> 2012 (73)	25	99 [97-99]	89 [84-92]
Prospectively ECG-triggered coronary CT angiography	Von Ballmoos <i>et al.</i> 2011 (74)	16	100 [98-100]	89 [82-89]
	Sun <i>et al.</i> 2012 (75)	14	99 [98-100]	91 [88-94]
	Sun <i>et al.</i> 2012 (76)	22	97.7 [93.7-100]	92.1 [87.2-97]
	Sabarudin <i>et al.</i> 2013 (77)	23	98.3 [96-100]	90.5 [85.7-96]
320-slice coronary CT angiography	Gaudio <i>et al.</i> 2013 (79)	7	95.4 [88.8-98.2]	94.7 [89.1-97.5]
	Li <i>et al.</i> 2013 (80)	10	93 [91-95]	86 [82-89]

CT, computed tomography; ECG, electrocardiogram.

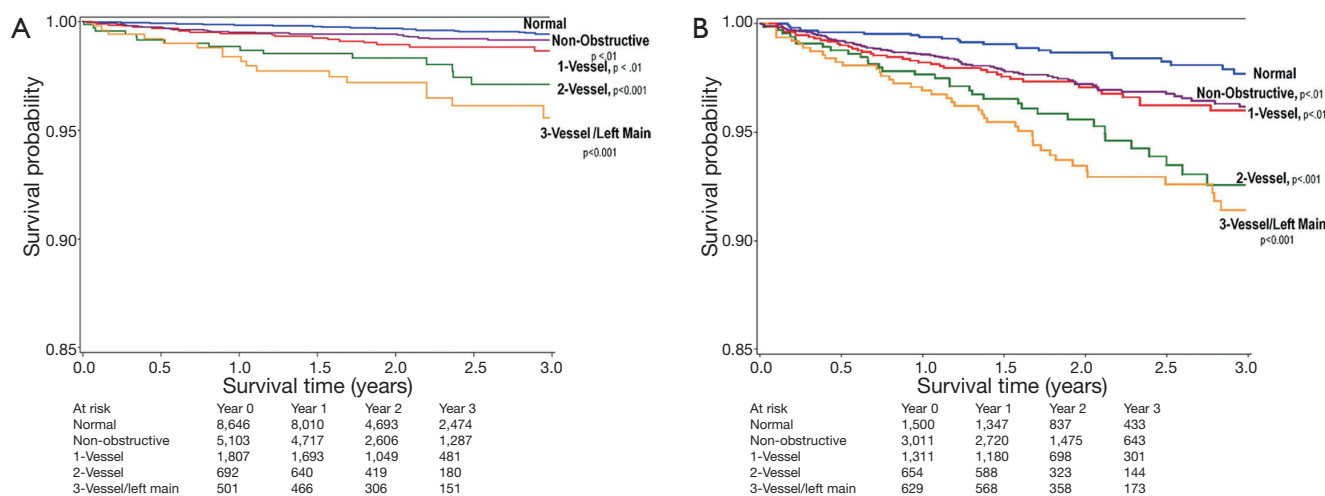


Figure 17 Unadjusted all-cause 3-year Kaplan-Meier survival by presence, extent, and severity of coronary artery disease by coronary CT angiography as stratified by age <65 or ≥65 years. Although rates of mortality in relationship coronary artery disease extent are lower in patients age <65 years (A), patients age <65 years with 2- and 3-vessel coronary artery disease experience a higher relative rate of mortality referenced to patients age <65 years with no coronary artery disease in comparison with patients age ≥65 years with 2- and 3-vessel coronary artery disease referenced to patients age ≥65 years with no coronary artery disease (B). Reprint with permission from ref (91). CT, computed tomography.

Currently, there are three multicentre trials, namely DISCOVER-FLOW (Diagnosis of Ischemia-Causing Coronary Stenoses by Noninvasive FFR Computed from Coronary Computed Tomographic Angiograms, conducted at four sites in three countries including Korea, Latvia and USA), DeFACTO (Determination of Fractional Flow Reserve by Anatomic Computed Tomographic Angiography, conducted at 17 centres in 5 countries including Belgium,

Canada, Korea, Latvia and USA) and NXT (NeXt sTeps, conducted at 10 centres in 7 countries including Australia, Denmark, Germany, Japan, Korea, Latvia and the UK) investigating the diagnostic value of FFRCT in coronary artery disease (94-96). On a per-patient analysis, diagnostic sensitivity and specificity of FFRCT ranged from 86-90% and 54-79%, while on a per-vessel analysis, diagnostic sensitivity and specificity of FFRCT were 84% and 86-

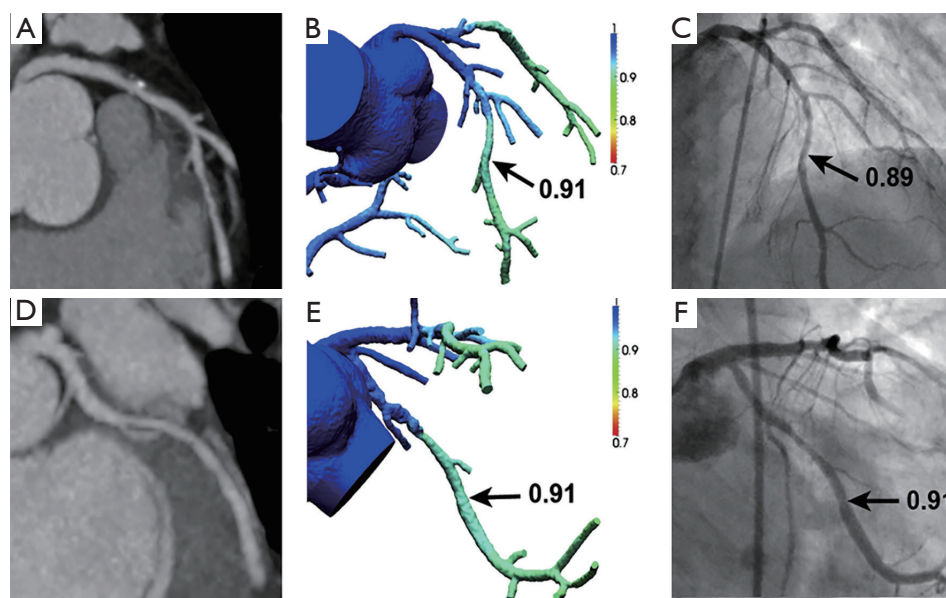


Figure 18 Fractional flow reserve (FFR) derived from computed tomography (CT) angiography (FFR_{CT}) results for 66-year-old man with multivessel coronary artery disease but no lesion-specific ischemia. (A) Coronary computed tomography angiography (CCTA) demonstrating stenosis in the left anterior descending coronary artery (LAD); (B) FFR_{CT} demonstrates no ischemia in the LAD, with a computed value of 0.91; (C) invasive coronary angiography (ICA) with FFR also demonstrates no ischemia in the LAD, with a measured value of 0.89; (D) CCTA demonstrating stenosis in the left circumflex coronary (LCx) artery; (E) FFR_{CT} demonstrates no ischemia in the LCx, with a computed value of 0.91; (F) ICA with FFR also demonstrates no ischemia in the LCx, with a measured value of 0.91. Reprint with permission from ref (92).

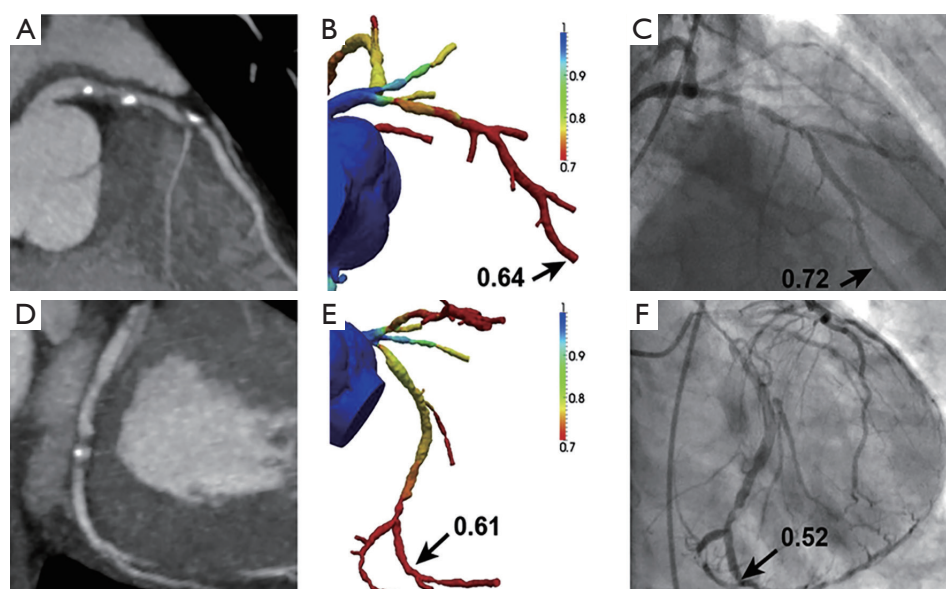


Figure 19 FFR_{CT} results for 66-year-old man with multivessel coronary artery disease and lesion-specific ischemia. (A) Coronary CT angiography (CCTA) demonstrating stenosis in the left anterior descending coronary artery (LAD); (B) FFR_{CT} demonstrates ischemia in the LAD, with a computed value of 0.64; (C) invasive coronary angiography (ICA) with FFR also demonstrates ischemia in the LAD, with a measured value of 0.72; (D) CCTA demonstrating stenosis in the left circumflex (LCx); (E) FFR_{CT} demonstrates ischemia in the LCx, with a computed value of 0.61; (F) ICA with FFR also demonstrates ischemia in the LCx, with a measured value of 0.52. Reprint with permission from ref (92). FFR_{CT} , fractional flow reserve (FFR) derived from coronary computed tomography (CT) angiography.

88%, respectively. The present findings support that FFRCT is superior to CCTA for the diagnosis of ischemia-causing lesions on both per-patient and per-vessel analysis as determined by an invasive FFR the reference standard. However, more multicentre trials need to be performed to compare the clinical impact of FFRCT guided versus standard diagnostic evaluation on clinical outcomes, costs and quality of life in patients with suspected coronary artery disease.

CTA-radiation dose

It is a well-known fact that CT is associated with high radiation dose which has raised concerns in the medical field over the last decade. With increasing applications of CTA in the cardiovascular practice, the research focus has shifted from the previous emphasis on diagnostic value of CTA to the current focus on reduction of radiation dose with acceptable diagnostic image quality. This is reflected by implementing various dose-reduction strategies with effective outcomes having been achieved.

CTA is commonly used as the gold standard of surveillance in patients following EVAR of AAA. However, excessive dependence on CT is expensive and exposes the patients to nephrotoxic intravenous contrast and ionizing radiation (97,98). Increasing the proportional use of non-nephrotoxic imaging modalities after EVAR has been advocated as an alternative approach to reduce surveillance-related morbidity (99). On the basis of 5-year follow-up outcomes, Sternbergh *et al.* proposed a modified surveillance protocol to alter the intensity and frequency of postoperative imaging follow-up. In patients without early endoleaks, the 6-month surveillance is eliminated, and the yearly aortic ultrasound examination is recommended for long-term surveillance of more than 1 year (100). There is increasing evidence of a trend from using conventional CT follow-up to ultrasound monitoring (100,101), so there is a need for a contemporary evaluation of surveillance after EVAR. A survey involving 41 clinical centres experienced in EVAR in the UK has shown there is significant heterogeneity in national practice for postoperative surveillance after EVAR (102). Intensive use of CT was observed in some centres and this may lead to cumulative renal injury due to repeated administration of contrast agents and radiation exposure. A recent study concluded that contrast-enhanced ultrasound is as accurate as CTA in monitoring endoleaks, aneurysm sac diameters, and target vessel patency in patients treated with fenestrated stent grafts (103).

The increased use of CTPA, especially in young patients with suspected PE raises concerns about the risk of radiation-induced malignancy and developing contrast-induced nephrotoxicity. Low radiation dose CTPA protocols with low contrast volume are increasingly studied due to the advantages of reducing radiation dose and minimising the risk of contrast-induced nephropathy (104-108). Low tube voltage and high pitch protocols have been reported to be effective approaches for reduction of radiation dose and contrast volume during CTPA examinations. Studies reported that using 80 kVp in CTPA can reduce radiation dose by 40% and contrast volume by 25% without compromising image quality (109,110). IR is a recently introduced algorithm which has been shown to reduce image noise and improve image quality while significantly reducing radiation dose in CT scans (111-113). High-pitch CTPA with low kVp combined with IR has been reported in recent studies to show that radiation dose is reduced by 52%, with contrast volume of 20 mL used in low-dose protocol (114,115). Another strategy on dose reduction is the application of dual-energy CT (DECT) which allows material decomposition of soft tissue, iodine and air within the chest CT scan. DECT has been shown to reduce patient dose by 28% compared with single-source CT while improving image visualisation of pulmonary vessels and diagnostic confidence (116,117). Further studies will provide more evidence of the clinical impact of DECT on CTPA (118).

High radiation dose associated with CCTA is well recognised in the literature, with significant progress having been made over the last decade on dose reduction during CCTA examinations. The commonly used dose-reduction strategies include ECG-controlled tube current modulation, adjustment of kVp values based on patient's body mass index, high-pitch CCTA protocols, prospectively ECG-triggered CCTA, and use of IR algorithms (74-77,119-128). With use of these approaches, radiation dose can be reduced by more than 80% from initially 20 mSv to about 2 mSv while still maintaining high level of diagnostic accuracy. Currently, the low-dose CCTA protocols are increasingly used in clinical practice with dose similar to or even lower than of invasive coronary angiography. Dose of less than 1 mSv are already achievable with the current CT scanners, while ultra-low-dose CCTA has been reported in a recent study with the mean radiation dose of 0.29 mSv, which is comparable to a chest x-ray examination in two views (*Figure 20*) (129). These technical developments confirm that this technique has become a more attractive alternative to

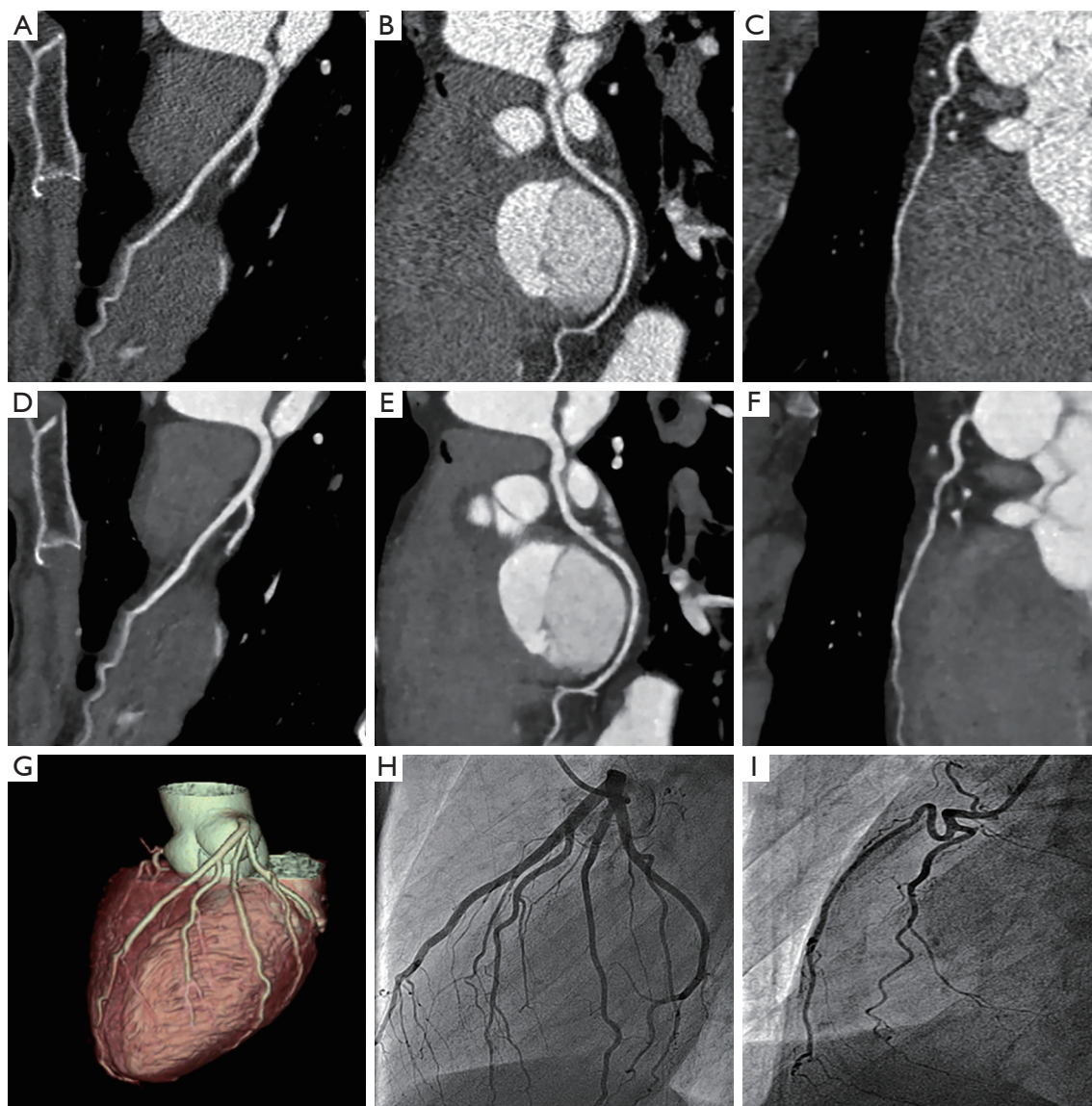


Figure 20 Normal coronary arteries. Images of normal coronary arteries in a 53-year-old patient (body mass index 17 kg/m^2) by coronary CT angiography with 0.19 mSv . Images without model-based iterative reconstruction algorithm (MBIR): (A) left anterior descending; (B) left circumflex; and (C) right coronary artery. Images with MBIR: (D) left anterior descending; (E) left circumflex; and (F) right coronary artery; (G) three-dimensional volume-rendered computed tomography image. (H and I) Invasive coronary angiography confirming normal left and right coronary vessels. Reprint with permission from ref (129). CT, computed tomography.

invasive coronary angiography.

Summary and concluding remarks

CT angiography represents the most important development in CT imaging, and it has evolved from the initial role of serving as a supplementary modality to an essential tool that plays an important role in the diagnosis

and management of cardiovascular disease which involves arterial system in the body. Technological advancements in CT data acquisition and image processing techniques have enabled this technique to become a routine imaging modality in daily clinical practice. With emergence of novel CT scanner geometries, advanced data reconstruction and postprocessing techniques, CT angiography will continue to play a dominant role in the diagnosis of cardiovascular

disease, prediction of disease extent and assistance of clinicians in effective patient management.

Disclosure: The authors declare no conflict of interest.

References

1. Sun Z, Mwipatayi BP, Allen YB, Hartley DE, Lawrence-Brown MM. Multislice CT angiography of fenestrated endovascular stent grafting for treating abdominal aortic aneurysms: a pictorial review of the 2D/3D visualizations. *Korean J Radiol* 2009;10:285-93.
2. Castañer E, Andreu M, Gallardo X, Mata JM, Cabezuelo MA, Pallardó Y. CT in nontraumatic acute thoracic aortic disease: typical and atypical features and complications. *Radiographics* 2003;23 Spec No:S93-110.
3. Sebastià C, Pallisa E, Quiroga S, Alvarez-Castells A, Dominguez R, Evangelista A. Aortic dissection: diagnosis and follow-up with helical CT. *Radiographics* 1999;19:45-60; quiz 149-50.
4. Schoepf UJ, Goldhaber SZ, Costello P. Spiral computed tomography for acute pulmonary embolism. *Circulation* 2004;109:2160-7.
5. Perrier A, Roy PM, Sanchez O, Le Gal G, Meyer G, Gourdièr AL, Furber A, Revel MP, Howarth N, Davido A, Bounameaux H. Multidetector-row computed tomography in suspected pulmonary embolism. *N Engl J Med* 2005;352:1760-8.
6. Sun Z, Jiang W. Diagnostic value of multislice computed tomography angiography in coronary artery disease: a meta-analysis. *Eur J Radiol* 2006;60:279-86.
7. Sun Z, Lin C, Davidson R, Dong C, Liao Y. Diagnostic value of 64-slice CT angiography in coronary artery disease: a systematic review. *Eur J Radiol* 2008;67:78-84.
8. Vanhoenacker PK, Heijenbrok-Kal MH, Van Heste R, Decramer I, Van Hoe LR, Wijns W, Hunink MG. Diagnostic performance of multidetector CT angiography for assessment of coronary artery disease: meta-analysis. *Radiology* 2007;244:419-28.
9. Abdulla J, Abildstrom SZ, Gotzsche O, Christensen E, Kober L, Torp-Pedersen C. 64-multislice detector computed tomography coronary angiography as potential alternative to conventional coronary angiography: a systematic review and meta-analysis. *Eur Heart J* 2007;28:3042-50.
10. Stein PD, Yaekoub AY, Matta F, Sostman HD. 64-slice CT for diagnosis of coronary artery disease: a systematic review. *Am J Med* 2008;121:715-25.
11. Mowatt G, Cook JA, Hillis GS, Walker S, Fraser C, Jia X, Waugh N. 64-Slice computed tomography angiography in the diagnosis and assessment of coronary artery disease: systematic review and meta-analysis. *Heart* 2008;94:1386-93.
12. Sun Z. Cardiac CT imaging in coronary artery disease: Current status and future directions. *Quant Imaging Med Surg* 2012;2:98-105.
13. Sun Z, Choo GH, Ng KH. Coronary CT angiography: current status and continuing challenges. *Br J Radiol* 2012;85:495-510.
14. Guo SL, Guo YM, Zhai YN, Ma B, Wang P, Yang KH. Diagnostic accuracy of first generation dual-source computed tomography in the assessment of coronary artery disease: a meta-analysis from 24 studies. *Int J Cardiovasc Imaging* 2011;27:755-71.
15. Pelliccia F, Pasceri V, Evangelista A, Pergolini A, Barilla F, Viceconte N, Tanzilli G, Schiariti M, Greco C, Gaudio C. Diagnostic accuracy of 320-row computed tomography as compared with invasive coronary angiography in unselected, consecutive patients with suspected coronary artery disease. *Int J Cardiovasc Imaging* 2013;29:443-52.
16. Rozenblit AM, Patlas M, Rosenbaum AT, Okhi T, Veith FJ, Laks MP, Ricci ZJ. Detection of endoleaks after endovascular repair of abdominal aortic aneurysm: value of unenhanced and delayed helical CT acquisitions. *Radiology* 2003;227:426-33.
17. Armerding MD, Rubin GD, Beaulieu CF, Slonim SM, Olcott EW, Samuels SL, Jorgensen MJ, Semba CP, Jeffrey RB Jr, Dake MD. Aortic aneurysmal disease: assessment of stent-graft treatment-CT versus conventional angiography. *Radiology* 2000;215:138-46.
18. Stavropoulos SW, Clark TW, Carpenter JP, Fairman RM, Litt H, Velazquez OC, Insko E, Farner M, Baum RA. Use of CT angiography to classify endoleaks after endovascular repair of abdominal aortic aneurysms. *J Vasc Interv Radiol* 2005;16:663-7.
19. Sun Z. Helical CT angiography of abdominal aortic aneurysms treated with suprarenal stent grafting. *Cardiovasc Intervent Radiol* 2003;26:290-5.
20. Rydberg J, Kopecky KK, Lalka SG, Johnson MS, Dalsing MC, Persohn SA. Stent grafting of abdominal aortic aneurysms: pre-and postoperative evaluation with multislice helical CT. *J Comput Assist Tomogr* 2001;25:580-6.
21. Sun Z, Ng KH. Multislice CT angiography in cardiac imaging. Part III: radiation risk and dose reduction. *Singapore Med J* 2010;51:374-80.

22. Sun ZH. Abdominal aortic aneurysm: Treatment options, image visualizations and follow-up procedures. *J Geriatr Cardiol* 2012;9:49-60.
23. Sun Z, Squelch A, Bartlett A, Cunningham K, Lawrence-Brown M. 3D stereoscopic visualization of fenestrated stent grafts. *Cardiovasc Intervent Radiol* 2009;32:1053-8.
24. Tam MD, Laycock SD, Brown JR, Jakeways M. 3D printing of an aortic aneurysm to facilitate decision making and device selection for endovascular aneurysm repair in complex neck anatomy. *J Endovasc Ther* 2013;20:863-7.
25. Ihara T, Komori K, Yamamoto K, Kobayashi M, Banno H, Kodama A. Three-dimensional workstation is useful for measuring the correct size of abdominal aortic aneurysm diameters. *Ann Vasc Surg* 2013;27:154-61.
26. Mora C, Marcus C, Barbe C, Ecarnot F, Long A. Measurement of maximum diameter of native abdominal aortic aneurysm by angio-CT: reproducibility is better with the semi-automated method. *Eur J Vasc Endovasc Surg* 2014;47:139-50.
27. Kontopodis N, Metaxa E, Gionis M, Papaharilaou Y, Ioannou CV. Discrepancies in determination of abdominal aortic aneurysms maximum diameter and growth rate, using axial and orthogonal computed tomography measurements. *Eur J Radiol* 2013;82:1398-403.
28. Greenhalgh RM, Brown LC, Kwong GP, Powell JT, Thompson SG; EVAR trial participants. Comparison of endovascular aneurysm repair with open repair in patients with abdominal aortic aneurysm (EVAR trial 1), 30-day operative mortality results: randomised controlled trial. *Lancet* 2004;364:843-8.
29. Brown LC, Greenhalgh RM, Thompson SG, Powell JT; EVAR Trial Participants. Does EVAR alter the rate of cardiovascular events in patients with abdominal aortic aneurysm considered unfit for open repair? Results from the randomised EVAR trial 2. *Eur J Vasc Endovasc Surg* 2010;39:396-402.
30. Prinssen M, Verhoeven EL, Buth J, Cuypers PW, van Sambeek MR, Balm R, Buskens E, Grobbee DE, Blankensteijn JD; Dutch Randomized Endovascular Aneurysm Management (DREAM) Trial Group. A randomized trial comparing conventional and endovascular repair of abdominal aortic aneurysms. *N Engl J Med* 2004;351:1607-18.
31. EVAR trial participants. Endovascular aneurysm repair and outcome in patients unfit for open repair of abdominal aortic aneurysm (EVAR trial 2): randomised controlled trial. *Lancet* 2005;365:2187-92.
32. Schouten O, Lever TM, Welten GM, Winkel TA, Dols LF, Bax JJ, van Domburg RT, Verhagen HJ, Poldermans D. Long-term cardiac outcome in high-risk patients undergoing elective endovascular or open infrarenal abdominal aortic aneurysm repair. *Eur J Vasc Endovasc Surg* 2008;36:646-52.
33. Yeung KK, van der Laan MJ, Wever JJ, van Waes PF, Blankensteijn JD. New post-imaging software provides fast and accurate volume data from CTA surveillance after endovascular aneurysm repair. *J Endovasc Ther* 2003;10:887-93.
34. Wever JJ, Blankensteijn JD, van Rijn JC, Broeders IA, Eikelboom BC, Mali WP. Inter- and intraobserver variability of CT measurements obtained after endovascular repair of abdominal aortic aneurysms. *AJR Am J Roentgenol* 2000;175:1279-82.
35. van Prehn J, van der Wal MB, Vincken K, Bartels LW, Moll FL, van Herwaarden JA. Intra- and interobserver variability of aortic aneurysm volume measurement with fast CTA postprocessing software. *J Endovasc Ther* 2008;15:504-10.
36. Görlich J, Rilinger N, Sokiranski R, Orend KH, Ermis C, Krämer SC, Brambs HJ, Sunder-Plassmann L, Pamler R. Leakages after endovascular repair of aortic aneurysms: classification based on findings at CT, angiography, and radiography. *Radiology* 1999;213:767-72.
37. McWilliams RG, Martin J, White D, Gould DA, Rowlands PC, Haycox A, Brennan J, Gilling-Smith GL, Harris PL. Detection of endoleak with enhanced ultrasound imaging: comparison with biphasic computed tomography. *J Endovasc Ther* 2002;9:170-9.
38. Iezzi R, Cotroneo AR, Filippone A, Santoro M, Basilico R, Storto ML. Multidetector-row computed tomography angiography in abdominal aortic aneurysm treated with endovascular repair: evaluation of optimal timing of delayed phase imaging for the detection of low-flow endoleaks. *J Comput Assist Tomogr* 2008;32:609-15.
39. Sawhney R, Kerlan RK, Wall SD, Chuter TA, Ruiz DE, Canto CJ, LaBerge JM, Reilly LM, Yee J, Wilson MW, Jean-Claude J, Faruqi RM, Gordon RL. Analysis of initial CT findings after endovascular repair of abdominal aortic aneurysm. *Radiology* 2001;220:157-60.
40. Sun Z. Three-dimensional visualization of suprarenal aortic stent-grafts: evaluation of migration in midterm follow-up. *J Endovasc Ther* 2006;13:85-93.
41. Kalliafas S, Albertini JN, Macierewicz J, Yusuf SW, Whitaker SC, Davidson I, Hopkinson BR. Stent-graft migration after endovascular repair of abdominal aortic aneurysm. *J Endovasc Ther* 2002;9:743-7.

42. Sun Z, Winder RJ, Kelly BE, Ellis PK, Hirst DG. CT virtual intravascular endoscopy of abdominal aortic aneurysms treated with suprarenal endovascular stent grafting. *Abdom Imaging* 2003;28:580-7.
43. Sun Z, Winder RJ, Kelly BE, Ellis PK, Kennedy PT, Hirst DG. Diagnostic value of CT virtual intravascular endoscopy in aortic stent-grafting. *J Endovasc Ther* 2004;11:13-25.
44. Sun Z, O'Donnell ME, Winder RJ, Ellis PK, Blair PH. Effect of suprarenal fixation of aortic stent-grafts on the renal artery ostia: assessment of morphological changes by virtual intravascular endoscopy. *J Endovasc Ther* 2007;14:650-60.
45. Sun Z, Allen YB, Nadkarni S, Knight R, Hartley DE, Lawrence-Brown MM. CT virtual intravascular endoscopy in the visualization of fenestrated stent-grafts. *J Endovasc Ther* 2008;15:42-51.
46. Sun Z, Zheng H. Effect of suprarenal stent struts on the renal artery with ostial calcification observed on CT virtual intravascular endoscopy. *Eur J Vasc Endovasc Surg* 2004;28:534-42.
47. Golledge J, Eagle KA. Acute aortic dissection. *Lancet* 2008;372:55-66.
48. Rampoldi V, Trimarchi S, Eagle KA, Nienaber CA, Oh JK, Bossone E, Myrmet T, Sangiorgi GM, De Vincentiis C, Cooper JV, Fang J, Smith D, Tsai T, Raghupathy A, Fattori R, Sechtem U, Deeb MG, Sundt TM 3rd, Isselbacher EM; International Registry of Acute Aortic Dissection (IRAD) Investigators. Simple risk models to predict surgical mortality in acute type A aortic dissection: the International Registry of Acute Aortic Dissection score. *Ann Thorac Surg* 2007;83:55-61.
49. Nienaber CA, Fattori R, Mehta RH, Richartz BM, Evangelista A, Petzsch M, Cooper JV, Januzzi JL, Ince H, Sechtem U, Bossone E, Fang J, Smith DE, Isselbacher EM, Pape LA, Eagle KA; International Registry of Acute Aortic Dissection. Gender-related differences in acute aortic dissection. *Circulation* 2004;109:3014-21.
50. Hagan PG, Nienaber CA, Isselbacher EM, Bruckman D, Karavite DJ, Russman PL, Evangelista A, Fattori R, Suzuki T, Oh JK, Moore AG, Malouf JF, Pape LA, Gaca C, Sechtem U, Lenferink S, Deutsch HJ, Diedrichs H, Marcos y Robles J, Llovet A, Gilon D, Das SK, Armstrong WF, Deeb GM, Eagle KA. The International Registry of Acute Aortic Dissection (IRAD): new insights into an old disease. *JAMA* 2000;283:897-903.
51. Shiga T, Wajima Z, Apfel CC, Inoue T, Ohe Y. Diagnostic accuracy of transesophageal echocardiography, helical computed tomography, and magnetic resonance imaging for suspected thoracic aortic dissection: systematic review and meta-analysis. *Arch Intern Med* 2006;166:1350-6.
52. Sun Z, Cao Y. Multislice CT virtual intravascular endoscopy of aortic dissection: A pictorial essay. *World J Radiol* 2010;2:440-8.
53. Chirillo F, Salvador L, Bacchion F, Grisolia EF, Valfrè C, Olivari Z. Clinical and anatomical characteristics of subtle-discrete dissection of the ascending aorta. *Am J Cardiol* 2007;100:1314-9.
54. Fallenberg M, Juergens KU, Wichter T, Scheld HH, Fischbach R. Coronary artery aneurysm and type-A aortic dissection demonstrated by retrospectively ECG-gated multislice spiral CT. *Eur Radiol* 2002;12:201-4.
55. Murayama T, Funabashi N, Uehara M, Takaoka H, Komuro I. New classification of aortic dissection during the cardiac cycle as pulsating type and static type evaluated by electrocardiogram-gated multislice CT. *Int J Cardiol* 2010;142:177-86.
56. Ganten MK, Weber TF, von Tengg-Kobligk H, Böckler D, Stiller W, Geisbüsch P, Kauffmann GW, Delorme S, Bock M, Kauczor HU. Motion characterization of aortic wall and intimal flap by ECG-gated CT in patients with chronic B-dissection. *Eur J Radiol* 2009;72:146-53.
57. Weber TF, Ganten MK, Böckler D, Geisbüsch P, Kopp-Schneider A, Kauczor HU, von Tengg-Kobligk H. Assessment of thoracic aortic conformational changes by four-dimensional computed tomography angiography in patients with chronic aortic dissection type b. *Eur Radiol* 2009;19:245-53.
58. Yang S, Li X, Chao B, Wu L, Cheng Z, Duan Y, Wu D, Zhan Y, Chen J, Liu B, Ji X, Nie P, Wang X. Abdominal aortic intimal flap motion characterization in acute aortic dissection: assessed with retrospective ECG-gated thoracoabdominal aorta dual-source CT angiography. *PLoS One* 2014;9:e87664.
59. DiMusto PD, Williams DM, Patel HJ, Trimarchi S, Eliason JL, Upchurch GR Jr. Endovascular management of type B aortic dissections. *J Vasc Surg* 2010;52:26S-36S.
60. Lombardi JV, Cambria RP, Nienaber CA, Chiesa R, Teebken O, Lee A, Mossop P, Bharadwaj P; STABLE investigators. Prospective multicenter clinical trial (STABLE) on the endovascular treatment of complicated type B aortic dissection using a composite device design. *J Vasc Surg* 2012;55:629-40.
61. Melissano G, Bertoglio L, Rinaldi E, Civilini E, Tshomba Y, Kahlberg A, Agricola E, Chiesa R. Volume changes in aortic true and false lumen after the "PETTICOAT"

- procedure for type B aortic dissection. *J Vasc Surg* 2012;55:641-51.
62. Mayo J, Thakur Y. Pulmonary CT angiography as first-line imaging for PE: image quality and radiation dose considerations. *AJR Am J Roentgenol* 2013;200:522-8.
 63. Wittram C. How I do it: CT pulmonary angiography. *AJR Am J Roentgenol* 2007;188:1255-61.
 64. den Exter PL, van der Hulle T, Klok FA, Huisman MV. Advances in the diagnosis and management of acute pulmonary embolism. *Thromb Res* 2014;133 Suppl 2:S10-6.
 65. Righini M, Le Gal G, Aujesky D, Roy PM, Sanchez O, Verschuren F, Rutschmann O, Nonent M, Cornuz J, Thys F, Le Manach CP, Revel MP, Poletti PA, Meyer G, Mottier D, Perneger T, Bounameaux H, Perrier A. Diagnosis of pulmonary embolism by multidetector CT alone or combined with venous ultrasonography of the leg: a randomised non-inferiority trial. *Lancet* 2008;371:1343-52.
 66. Ghanima W, Almaas V, Aballi S, Dörje C, Niessen BE, Holmen LO, Almaas R, Abdelnoor M, Sandset PM. Management of suspected pulmonary embolism (PE) by D-dimer and multi-slice computed tomography in outpatients: an outcome study. *J Thromb Haemost* 2005;3:1926-32.
 67. Mos IC, Klok FA, Kroft LJ, DE Roos A, Dekkers OM, Huisman MV. Safety of ruling out acute pulmonary embolism by normal computed tomography pulmonary angiography in patients with an indication for computed tomography: systematic review and meta-analysis. *J Thromb Haemost* 2009;7:1491-8.
 68. Carrier M, Righini M, Wells PS, Perrier A, Anderson DR, Rodger MA, Pleasance S, Le Gal G. Subsegmental pulmonary embolism diagnosed by computed tomography: incidence and clinical implications. A systematic review and meta-analysis of the management outcome studies. *J Thromb Haemost* 2010;8:1716-22.
 69. Stein PD, Chenevert TL, Fowler SE, Goodman LR, Gottschalk A, Hales CA, Hull RD, Jablonski KA, Leeper KV Jr, Naidich DP, Sak DJ, Sostman HD, Tapson VF, Weg JG, Woodard PK; PIOPED III (Prospective Investigation of Pulmonary Embolism Diagnosis III) Investigators. Gadolinium-enhanced magnetic resonance angiography for pulmonary embolism: a multicenter prospective study (PIOPED III). *Ann Intern Med* 2010;152:434-43, W142-3.
 70. Revel MP, Sanchez O, Couchon S, Planquette B, Hernigou A, Niarra R, Meyer G, Chatellier G. Diagnostic accuracy of magnetic resonance imaging for an acute pulmonary embolism: results of the 'IRM-EP' study. *J Thromb Haemost* 2012;10:743-50.
 71. Sun Z, Dosari SA, Ng C, al-Muntashari A, Almaliky S. Multislice CT virtual intravascular endoscopy for assessing pulmonary embolisms: a pictorial review. *Korean J Radiol* 2010;11:222-30.
 72. Schoepf UJ, Costello P. CT angiography for diagnosis of pulmonary embolism: state of the art. *Radiology* 2004;230:329-37.
 73. Salavati A, Radmanesh F, Heidari K, Dwamena BA, Kelly AM, Cronin P. Dual-source computed tomography angiography for diagnosis and assessment of coronary artery disease: systematic review and meta-analysis. *J Cardiovasc Comput Tomogr* 2012;6:78-90.
 74. von Ballmoos MW, Haring B, Juillerat P, Alkadhi H. Meta-analysis: diagnostic performance of low-radiation-dose coronary computed tomography angiography. *Ann Intern Med* 2011;154:413-20.
 75. Sun Z, Ng KH. Diagnostic value of coronary CT angiography with prospective ECG-gating in the diagnosis of coronary artery disease: a systematic review and meta-analysis. *Int J Cardiovasc Imaging* 2012;28:2109-19.
 76. Sun Z, Ng KH. Prospective versus retrospective ECG-gated multislice CT coronary angiography: a systematic review of radiation dose and diagnostic accuracy. *Eur J Radiol* 2012;81:e94-100.
 77. Sabarudin A, Sun Z, Ng KH. Coronary computed tomography angiography with prospective electrocardiography triggering: a systematic review of image quality and radiation dose. *Singapore Med J* 2013;54:15-23.
 78. Sun Z, Xu L. Coronary CT Angiography in the Quantitative Assessment of Coronary Plaques. *Biomed Res Int* 2014;2014:346380.
 79. Gaudio C, Pelliccia F, Evangelista A, Tanzilli G, Paravati V, Pannarale G, Pannitteri G, Barilla F, Greco C, Franzoni F, Speziale G, Pasceri V. 320-row computed tomography coronary angiography vs. conventional coronary angiography in patients with suspected coronary artery disease: a systematic review and meta-analysis. *Int J Cardiol* 2013;168:1562-4.
 80. Li S, Ni Q, Wu H, Peng L, Dong R, Chen L, Liu J. Diagnostic accuracy of 320-slice computed tomography angiography for detection of coronary artery stenosis: meta-analysis. *Int J Cardiol* 2013;168:2699-705.
 81. Sun Z. Comment on: Diagnostic accuracy of 320-slice computed tomography angiography for detection of coronary artery stenosis: meta-analysis (*Int J Cardiol* 2013, <http://dx.doi.org/10.1016/j.ijcard.2013.03.023>). *Int J Cardiol* 2013;168:4895-6.

82. Liu YC, Sun Z, Tsay PK, Chan T, Hsieh IC, Chen CC, Wen MS, Wan YL. Significance of coronary calcification for prediction of coronary artery disease and cardiac events based on 64-slice coronary computed tomography angiography. *Biomed Res Int* 2013;2013:472347.
83. Chow BJ, Wells GA, Chen L, Yam Y, Galiwango P, Abraham A, Sheth T, Dennie C, Beanlands RS, Ruddy TD. Prognostic value of 64-slice cardiac computed tomography severity of coronary artery disease, coronary atherosclerosis, and left ventricular ejection fraction. *J Am Coll Cardiol* 2010;55:1017-28.
84. Miszalski-Jamka T, Klimeczek P, Banyś R, Krupiński M, Nycz K, Bury K, Lada M, Pelberg R, Kereiakes D, Mazur W. The composition and extent of coronary artery plaque detected by multislice computed tomographic angiography provides incremental prognostic value in patients with suspected coronary artery disease. *Int J Cardiovasc Imaging* 2012;28:621-31.
85. Andreini D, Pontone G, Mushtaq S, Bartorelli AL, Bertella E, Antonioli L, Formenti A, Cortinovis S, Veglia F, Annoni A, Agostoni P, Montorsi P, Ballerini G, Fiorentini C, Pepi M. A long-term prognostic value of coronary CT angiography in suspected coronary artery disease. *JACC Cardiovasc Imaging* 2012;5:690-701.
86. Sozzi FB, Civaia F, Rossi P, Robillon JF, Rusek S, Berthier F, Bourlon F, Iacuzio L, Dreyfus G, Dor V. Long-term follow-up of patients with first-time chest pain having 64-slice computed tomography. *Am J Cardiol* 2011;107:516-21.
87. Hadamitzky M, Täubert S, Deseive S, Byrne RA, Martinoff S, Schömig A, Hausleiter J. Prognostic value of coronary computed tomography angiography during 5 years of follow-up in patients with suspected coronary artery disease. *Eur Heart J* 2013;34:3277-85.
88. Dougoud S, Fuchs TA, Stehli J, Clerc OF, Buechel RR, Herzog BA, Leschka S, Alkadhi H, Kaufmann PA, Gaemperli O. Prognostic value of coronary CT angiography on long-term follow-up of 6.9 years. *Int J Cardiovasc Imaging* 2014;30:969-76.
89. Min JK, Lin FY, Dunning AM, Delago A, Egan J, Shaw LJ, Berman DS, Callister TQ. Incremental prognostic significance of left ventricular dysfunction to coronary artery disease detection by 64-detector row coronary computed tomographic angiography for the prediction of all-cause mortality: results from a two-centre study of 5330 patients. *Eur Heart J* 2010;31:1212-9.
90. Min JK, Feignoux J, Treutenaere J, Laperche T, Sablayrolles J. The prognostic value of multidetector coronary CT angiography for the prediction of major adverse cardiovascular events: a multicenter observational cohort study. *Int J Cardiovasc Imaging* 2010;26:721-8.
91. Min JK, Dunning A, Lin FY, Achenbach S, Al-Mallah M, Budoff MJ, Cademartiri F, Callister TQ, Chang HJ, Cheng V, Chinnaiyan K, Chow BJ, Delago A, Hadamitzky M, Hausleiter J, Kaufmann P, Maffei E, Raff G, Shaw LJ, Villines T, Berman DS; CONFIRM Investigators. Age- and sex-related differences in all-cause mortality risk based on coronary computed tomography angiography findings results from the International Multicenter CONFIRM (Coronary CT Angiography Evaluation for Clinical Outcomes: An International Multicenter Registry) of 23,854 patients without known coronary artery disease. *J Am Coll Cardiol* 2011;58:849-60.
92. Taylor CA, Fonte TA, Min JK. Computational fluid dynamics applied to cardiac computed tomography for noninvasive quantification of fractional flow reserve: scientific basis. *J Am Coll Cardiol* 2013;61:2233-41.
93. Zarins CK, Taylor CA, Min JK. Computed fractional flow reserve (FFRCT) derived from coronary CT angiography. *J Cardiovasc Transl Res* 2013;6:708-14.
94. Koo BK, Erglis A, Doh JH, Daniels DV, Jegere S, Kim HS, Dunning A, DeFrance T, Lansky A, Leipsic J, Min JK. Diagnosis of ischemia-causing coronary stenoses by noninvasive fractional flow reserve computed from coronary computed tomographic angiograms. Results from the prospective multicenter DISCOVER-FLOW (Diagnosis of Ischemia-Causing Stenoses Obtained Via Noninvasive Fractional Flow Reserve) study. *J Am Coll Cardiol* 2011;58:1989-97.
95. Min JK, Berman DS, Budoff MJ, Jaffer FA, Leipsic J, Leon MB, Mancini GB, Mauri L, Schwartz RS, Shaw LJ. Rationale and design of the DeFACTO (Determination of Fractional Flow Reserve by Anatomic Computed Tomographic Angiography) study. *J Cardiovasc Comput Tomogr* 2011;5:301-9.
96. Nørgaard BL, Leipsic J, Gaur S, Seneviratne S, Ko BS, Ito H, Jensen JM, Mauri L, De Bruyne B, Bezerra H, Osawa K, Marwan M, Naber C, Erglis A, Park SJ, Christiansen EH, Kaltoft A, Lassen JF, Bøtker HE, Achenbach S; NXT Trial Study Group. Diagnostic performance of noninvasive fractional flow reserve derived from coronary computed tomography angiography in suspected coronary artery disease: the NXT trial (Analysis of Coronary Blood Flow Using CT Angiography: Next Steps). *J Am Coll Cardiol* 2014;63:1145-55.
97. Michaels JA, Drury D, Thomas SM. Cost-effectiveness of

- endovascular abdominal aortic aneurysm repair. *Br J Surg* 2005;92:960-7.
98. Weerakkody RA, Walsh SR, Cousins C, Goldstone KE, Tang TY, Gaunt ME. Radiation exposure during endovascular aneurysm repair. *Br J Surg* 2008;95:699-702.
 99. Boyle JR. Long-term outcome of endovascular abdominal aortic aneurysm repair. *Br J Surg* 2009;96:447-8.
 100. Sternbergh WC 3rd, Greenberg RK, Chuter TA, Tonnessen BH; Zenith Investigators. Redefining postoperative surveillance after endovascular aneurysm repair: recommendations based on 5-year follow-up in the US Zenith multicenter trial. *J Vasc Surg* 2008;48:278-84; discussion 284-5.
 101. Sun Z. Diagnostic value of color duplex ultrasonography in the follow-up of endovascular repair of abdominal aortic aneurysm. *J Vasc Interv Radiol* 2006;17:759-64.
 102. Karthikesalingam A, Page AA, Pettengell C, Hinchliffe RJ, Loftus IM, Thompson MM, Holt PJ. Heterogeneity in surveillance after endovascular aneurysm repair in the UK. *Eur J Vasc Endovasc Surg* 2011;42:585-90.
 103. Perini P, Sediri I, Midulla M, Delsart P, Gautier C, Haulon S. Contrast-enhanced ultrasound vs. CT angiography in fenestrated EVAR surveillance: a single-center comparison. *J Endovasc Ther* 2012;19:648-55.
 104. Bolen MA, Renapurkar RD, Popovic ZB, Heresi GA, Flamm SD, Lau CT, Halliburton SS. High-pitch ECG-synchronized pulmonary CT angiography versus standard CT pulmonary angiography: a prospective randomized study. *AJR Am J Roentgenol* 2013;201:971-6.
 105. Co SJ, Mayo J, Liang T, Krzymyk K, Yousefi M, Nicolaou S. Iterative reconstructed ultra high pitch CT pulmonary angiography with cardiac bowtie-shaped filter in the acute setting: effect on dose and image quality. *Eur J Radiol* 2013;82:1571-6.
 106. De Zordo T, von Lutterotti K, Dejaco C, Soegner PF, Frank R, Aigner F, Klauser AS, Pechlaner C, Schoepf UJ, Jaschke WR, Feuchtner GM. Comparison of image quality and radiation dose of different pulmonary CTA protocols on a 128-slice CT: high-pitch dual source CT, dual energy CT and conventional spiral CT. *Eur Radiol* 2012;22:279-86.
 107. Faggioni L, Neri E, Sbragia P, Pascale R, D'Errico L, Caramella D, Bartolozzi C. 80-kV pulmonary CT angiography with 40 mL of iodinated contrast material in lean patients: comparison of vascular enhancement with iodixanol (320 mg I/mL) and iomeprol (400 mg I/mL). *AJR Am J Roentgenol* 2012;199:1220-5.
 108. Goble EW, Abdulkarim JA. CT pulmonary angiography using a reduced volume of high-concentration iodinated contrast medium and multiphasic injection to achieve dose reduction. *Clin Radiol* 2014;69:36-40.
 109. Szucs-Farkas Z, Kurmann L, Strautz T, Patak MA, Vock P, Schindera ST. Patient exposure and image quality of low-dose pulmonary computed tomography angiography: comparison of 100- and 80-kVp protocols. *Invest Radiol* 2008;43:871-6.
 110. Szucs-Farkas Z, Schaller C, Bensler S, Patak MA, Vock P, Schindera ST. Detection of pulmonary emboli with CT angiography at reduced radiation exposure and contrast material volume: comparison of 80 kVp and 120 kVp protocols in a matched cohort. *Invest Radiol* 2009;44:793-9.
 111. Leipsic J, Nguyen G, Brown J, Sin D, Mayo JR. A prospective evaluation of dose reduction and image quality in chest CT using adaptive statistical iterative reconstruction. *AJR Am J Roentgenol* 2010;195:1095-9.
 112. Singh S, Kalra MK, Gilman MD, Hsieh J, Pien HH, Digumarthy SR, Shepard JA. Adaptive statistical iterative reconstruction technique for radiation dose reduction in chest CT: a pilot study. *Radiology* 2011;259:565-73.
 113. Cornfeld D, Israel G, Detroy E, Bokhari J, Mojibian H. Impact of Adaptive Statistical Iterative Reconstruction (ASIR) on radiation dose and image quality in aortic dissection studies: a qualitative and quantitative analysis. *AJR Am J Roentgenol* 2011;196:W336-40.
 114. Lu GM, Luo S, Meinel FG, McQuiston AD, Zhou CS, Kong X, Zhao YE, Zheng L, Schoepf UJ, Zhang LJ. High-pitch computed tomography pulmonary angiography with iterative reconstruction at 80 kVp and 20 mL contrast agent volume. *Eur Radiol* 2014. [Epub ahead of print].
 115. McLaughlin PD, Liang T, Homiedan M, Louis LJ, O'Connell TW, Krzymyk K, Nicolaou S, Mayo JR. High pitch, low voltage dual source CT pulmonary angiography: assessment of image quality and diagnostic acceptability with hybrid iterative reconstruction. *Emerg Radiol* 2014. [Epub ahead of print].
 116. Sangwaiya MJ, Kalra MK, Sharma A, Halpern EF, Shepard JA, Digumarthy SR. Dual-energy computed tomographic pulmonary angiography: a pilot study to assess the effect on image quality and diagnostic confidence. *J Comput Assist Tomogr* 2010;34:46-51.
 117. Bauer RW, Kramer S, Renker M, Schell B, Larson MC, Beeres M, Lehnert T, Jacobi V, Vogl TJ, Kerl JM. Dose and image quality at CT pulmonary angiography-comparison of first and second generation dual-energy CT and 64-slice CT. *Eur Radiol* 2011;21:2139-47.

118. Mayo J, Thakur Y. Pulmonary CT angiography as first-line imaging for PE: image quality and radiation dose considerations. *AJR Am J Roentgenol* 2013;200:522-8.
119. Sabarudin A, Sun Z, Yusof AK. Coronary CT angiography with single-source and dual-source CT: comparison of image quality and radiation dose between prospective ECG-triggered and retrospective ECG-gated protocols. *Int J Cardiol* 2013;168:746-53.
120. Earls JP, Berman EL, Urban BA, Curry CA, Lane JL, Jennings RS, McCulloch CC, Hsieh J, Londt JH. Prospectively gated transverse coronary CT angiography versus retrospectively gated helical technique: improved image quality and reduced radiation dose. *Radiology* 2008;246:742-53.
121. Shuman WP, Branch KR, May JM, Mitsumori LM, Lockhart DW, Dubinsky TJ, Warren BH, Caldwell JH. Prospective versus retrospective ECG gating for 64-detector CT of the coronary arteries: comparison of image quality and patient radiation dose. *Radiology* 2008;248:431-7.
122. Xu L, Yang L, Zhang Z, Li Y, Fan Z, Ma X, Lv B, Yu W. Low-dose adaptive sequential scan for dual-source CT coronary angiography in patients with high heart rate: comparison with retrospective ECG gating. *Eur J Radiol* 2010;76:183-7.
123. Hohl C, Mühlenbruch G, Wildberger JE, Leidecker C, Süß C, Schmidt T, Günther RW, Mahnken AH. Estimation of radiation exposure in low-dose multislice computed tomography of the heart and comparison with a calculation program. *Eur Radiol* 2006;16:1841-6.
124. Achenbach S, Marwan M, Ropers D, Schepis T, Pflederer T, Anders K, Kuettner A, Daniel WG, Uder M, Lell MM. Coronary computed tomography angiography with a consistent dose below 1 mSv using prospectively electrocardiogram-triggered high-pitch spiral acquisition. *Eur Heart J* 2010;31:340-6.
125. Paul JF, Abada HT. Strategies for reduction of radiation dose in cardiac multislice CT. *Eur Radiol* 2007;17:2028-37.
126. Leipsic J, Labounty TM, Heilbron B, Min JK, Mancini GB, Lin FY, Taylor C, Dunning A, Earls JP. Adaptive statistical iterative reconstruction: assessment of image noise and image quality in coronary CT angiography. *AJR Am J Roentgenol* 2010;195:649-54.
127. Bittencourt MS, Schmidt B, Seltmann M, Muschiol G, Ropers D, Daniel WG, Achenbach S. Iterative reconstruction in image space (IRIS) in cardiac computed tomography: initial experience. *Int J Cardiovasc Imaging* 2011;27:1081-7.
128. Layritz C, Schmid J, Achenbach S, Ulzheimer S, Wuest W, May M, Ropers D, Klinghammer L, Daniel WG, Pflederer T, Lell M. Accuracy of prospectively ECG-triggered very low-dose coronary dual-source CT angiography using iterative reconstruction for the detection of coronary artery stenosis: comparison with invasive catheterization. *Eur Heart J Cardiovasc Imaging* 2014. pii: jeu113. [Epub ahead of print].
129. Stehli J, Fuchs TA, Bull S, Clerc OF, Possner M, Buechel RR, Gaemperli O, Kaufmann PA. Accuracy of Coronary CT Angiography Using a Submillisievert Fraction of Radiation Exposure: Comparison With Invasive Coronary Angiography. *J Am Coll Cardiol* 2014;64:772-80.

Cite this article as: Sun Z, Al Moudi M, Cao Y. CT angiography in the diagnosis of cardiovascular disease: A transformation in cardiovascular CT practice. *Quant Imaging Med Surg* 2014;4(5):376-396. doi: 10.3978/j.issn.2223-4292.2014.10.02